Generic Bistability in Creased Conical Surfaces

F. Lechenault and M. Adda-Bedia
Laboratoire de Physique Statistique, Ecole Normale Supérieure, UPMC Université Paris 06, Université Paris-Diderot, CNRS, 24 rue Lhomond, 75005 Paris, France
(Received 17 July 2015; published 1 December 2015)

The emerging field of mechanical metamaterials has sought inspiration in the ancient art of origami as archetypal deployable structures that carry geometric rigidity, exhibit exotic material properties, and are potentially scalable. A promising venue to introduce functionality consists in coupling the elasticity of the sheet and the kinematics of the folds. In this spirit, we introduce a scale-free, analytical description of a very general class of snap-through, bistable patterns of creases naturally occurring at the vertices of real origami that can be used as building blocks to program and actuate the overall shape of the decorated sheet. These switches appear at the simplest possible level of creasing and admit straightforward experimental realizations.

DOI: 10.1103/PhysRevLett.115.235501 PACS numbers: 81.05.Zx, 46.05.+b, 46.70.-p

Origami structures are usually seen as assemblies of rigid faces articulated around creases with hingelike behavior [1–4]. Their deployment and degrees of freedom are, thus, purely kinematic, resulting only from the geometry of the crease network. Such structures have received significant attention, in particular, from the aerospace industry [5,6]. However, real folded structures, usually engineered from paper, polymeric, or even metal sheets, can deform outside the creases [7,8]. In such situations, face bending competes with crease actuation in a morphogenetic way. In order to rationalize this interplay, we investigate the equilibrium shape of an infinite elastic sheet on which one or more straight radial creases meet at a single vertex. We find that these structures generically exhibit bistability, in the sense that they can snap through from one metastable configuration to another. The conical geometry of these surfaces resemble the ones studied in Refs. [9–11], except that they are decorated by radial creases around which they can fold. We will then refer to them as foldable cones (f cones).

When a crease is imprinted on an elastic sheet, the deformation of the resulting structure will mainly result from the competition between the flexural stiffness of the sheet and the hingelike stiffness of the crease [12]. This competition gives rise to a material length scale $L^* \equiv B/\kappa$, where B is the bending modulus of the sheet, and κ is the elastic constant associated with the torsional hinge formed by the crease. L^* scales with the thickness of the sheet, though with a material amplification factor [12]. When the typical size of the system is much smaller than L^*, the system behaves as a regular origami, with faces remaining mostly undeformed and creases actuating when submitted to stress. On the other hand, if the system is much larger than L^*, its response will be governed by the bending of the sheet, while the angles of the creases will essentially keep their rest value.

In the conical situation we are interested in, the relevant geometrical length scale is the radius R of the plate. Since the lateral size of the faces grows linearly with the radial distance to the center, one expects a transition from a hinge-mediated to a bending-mediated face shape at some finite distance from the vertex. Thus, in the limit of large system size $R \gg L^*$, the creases can be approximated by infinitely stiff hinges connecting flexural plates. It is this limit we investigate here, which corresponds physically to "macroscopic" situations requiring a very large-scale separation between the system size and the thickness.

Consider such "infinite" sheet crossed by an infinite crease ($R \gg L^*$), basically two half-planes forming a finite angle. If one lays this structure on a flat surface, with the wedge coming upwards and then presses on the crease with a point force, it will at some stage "jump" to a metastable state where the initial crease is "broken" into two non-aligned semi-infinite creases [Fig. 1(c)]. Such a property

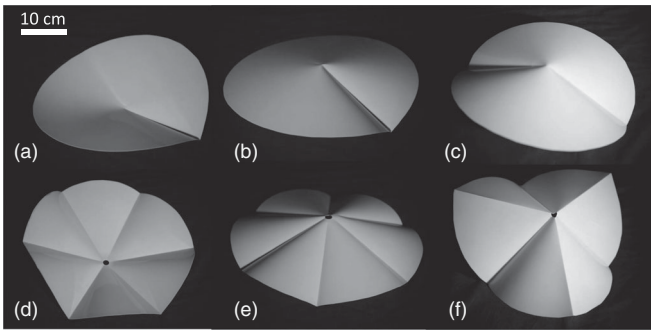

FIG. 1. Experimental, mechanically stable conical crease patterns, or f cones, in mylar-sheet disks (350 μm thick, 15 cm in radius, and $L^* \simeq 7$ cm [12]). (a),(b) Realizations of "semi-infinite" crease configurations that snap through one another. (c) "Infinite-crease" configuration obtained by snapping a straight-creased sheet. (d),(e) All-valley creases ($n = 6$) configurations that snap through one another. (f) Alternate mountain-valley crease configuration ($n = 6$). This configuration snaps into a mirror-symmetric, but rotated, state.

remains for an arbitrary number of evenly distributed radial "valley" creases, resulting in a pair of configurations that are not mirror symmetric [Figs. 1(d) and 1(e)]. Furthermore, this extends to a sheet decorated by an even number of evenly distributed alternating (valley or mountain) creases [Fig. 1(f)]. Experimental realizations of these structures prepared following the protocol detailed in Ref. [12] are mechanically metastable and simply lie on a tabletop (see Fig. 1).

We take advantage of the conical geometry of this problem to implement a scale-invariant description of these structures, thus, neglecting the possible complications associated with in-plane deformations and plasticity occurring near the vertex in real materials. In order to rationalize the corresponding shapes, or f cones, we consider an elastic sheet decorated with n evenly distributed straight creases meeting at a single vertex and with prescribed hinge angles between successive panels. We will focus on two generic fold configurations: the first one with equal opening angles all pointing in the same direction, which will be conventionally referred to as an all-valley creases f cone, and the second one with two different opening angles pointing in alternate directions, referred to as an alternate creases f cone. The general case of nonequal rest angles and nonequally spaced creases is formulated in Ref. [13].

We adopt a cylindrical coordinate system (ρ, θ) with the vertex located at $\rho = 0$ and $0 \le \theta \le \phi \equiv 2\pi/n$ to describe a slice of angular opening ϕ bounded by two creases. Following Ref. [14], an initially planar sheet described by a vector $\rho\hat{\rho}$ is deformed into $\vec{r} = \rho\hat{\rho} + u_\rho(\rho,\theta)\hat{\rho} + u_\theta(\rho,\theta)\hat{\theta} + \xi(\rho,\theta)\hat{z}$ with u_ρ, u_θ, and ξ the radial, azimuth, and axial displacements, respectively. The scale-invariant solutions we seek impose $\xi = \rho\psi(\theta)$. Requiring that the stretching strain vanishes in the limit of small deflections imposes [14]

$$u_\rho(\rho,\theta) = -\frac{\rho}{2}\psi^2(\theta), \tag{1}$$

$$u_\theta(\rho,\theta) = \frac{\rho}{2}\int^\theta d\theta[\psi^2(\theta) - \psi'^2(\theta)]. \tag{2}$$

Inextensibility in the azimuthal direction imposes

$$u_\theta(\rho,\phi) - u_\theta(\rho,0) = 0. \tag{3}$$

Finding the equilibrium shape of the creased sheet amounts to extremizing the following Lagrangian,

$$\mathcal{L}[\psi] = \frac{B}{2\rho}\left[\int_0^\phi d\theta[\psi(\theta) + \psi''(\theta)]^2 + \lambda\int_0^\phi d\theta[\psi^2(\theta) - \psi'^2(\theta)]\right], \tag{4}$$

where the first integral term is the bending energy density (per unit radius), and the second one enforces condition (3) through the Lagrange multiplier λ. Variation of Eq. (4) yields

$$\delta\mathcal{L}[\psi] = [(\psi + \psi'')\delta\psi']_0^\phi - [(\mu^2\psi' + \psi''')\delta\psi]_0^\phi + \int_0^\phi d\theta\delta\psi\left[\frac{d^2}{d\theta^2} + \mu^2\right]\left[\frac{d^2}{d\theta^2} + 1\right]\psi(\theta), \tag{5}$$

where $\mu^2 \equiv 1 + \lambda$. The resulting Euler-Lagrange equation reads

$$\left(\frac{d^2}{d\theta^2} + \mu^2\right)\left(\frac{d^2}{d\theta^2} + 1\right)\psi = 0. \tag{6}$$

Our modeling of a crease as an infinitely stiff hinge and the rotational symmetry of the structure around the z axis impose the boundary slopes but leave the deflections at the edges undetermined. Therefore, the boundary terms in Eq. (5) yield the following conditions:

$$\delta\psi'(0) = \delta\psi'(\phi) = 0, \tag{7}$$

$$\mu^2\psi'(0) + \psi'''(0) = \mu^2\psi'(\phi) + \psi'''(\phi) = 0. \tag{8}$$

Finally, it is important to recall that the Lagrange multiplier λ is related to the hoop stress through

$$\sigma_{\theta\theta} = -\frac{B\lambda}{h\rho^2}, \tag{9}$$

where h is the thickness of the plate [14]. Therefore $\lambda > 0$ (resp. $\lambda < 0$) corresponds to a compressive (resp. tensile) hoop stress.

All-valley creases f cone.—When all opening angles point in the same direction, the boundary conditions (7) read

$$\psi'(0) = -\psi'(\phi) = p, \tag{10}$$

where the constant p is the local slope of the crease with respect to the horizontal plane. Solving Eq. (6) with boundary conditions (8) and (10) yields

$$\psi(\theta) = p\frac{\cos\mu(\phi/2 - \theta)}{\mu\sin\mu\phi/2}. \tag{11}$$

The inextensibility condition (3) reads

$$(1 - \mu^2)\mu\phi + (1 + \mu^2)\sin\mu\phi = 0. \tag{12}$$

Noting that $\lambda = \mu^2 - 1$ can be arbitrarily negative, μ can be either real or purely imaginary. Solving Eq. (12) numerically yields two solutions μ_n^+ and $i\mu_n^-$ ($\mu_n^\pm > 0$) for all $n \ge 1$ (see Fig. 2), which correspond, respectively, to normalized axial displacements given by

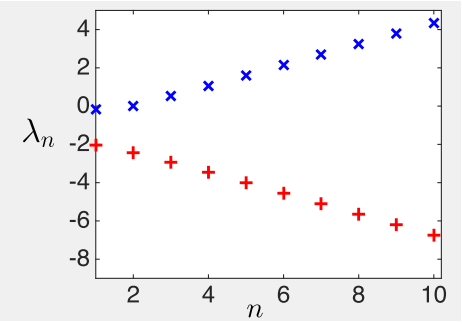

FIG. 2 (color online). Numerical solutions of Eq. (3) for the Lagrange multipliers λ_n^+ (×) and λ_n^- (+) as a function of the number of faces n. When $\lambda = \mu^2 + 1 > 0$ (resp. $\lambda < 0$), the structure is in compression (resp. tension).

$$\psi_n^+(\theta) = p\frac{\cos\mu_n^+(\pi/n-\theta)}{\mu_n^+\sin\mu_n^+\pi/n}, \tag{13}$$

$$\psi_n^-(\theta) = p\frac{\cosh\mu_n^-(\pi/n-\theta)}{\mu_n^-\sinh\mu_n^-\pi/n}. \tag{14}$$

We will now investigate specific situations starting from the single semi-infinite crease ($n = 1$). In this case, one has $\lambda_1^+ \simeq -0.15$ and $\lambda_1^- \simeq -2.04$ corresponding to the shapes shown in Figs. 3(a) and 3(b), respectively. Moreover, the associated hoop stresses are positive [see Eq. (9)]: both structures are in tension. The bending energy density for these states is $\mathcal{E}_1^+ = 1.30(Bp^2/2\rho)$ and $\mathcal{E}_1^- = 4.01(Bp^2/2\rho)$; the latter is, thus, metastable, and, hence, by definition corresponds to the "snapped" state.

The case $n = 2$ is marginal: the infinite crease configuration is stress free ($\lambda_2^+ = 0$) and, thus, devoid of curvature. The deflection admits the simple expression $\psi_2^+(\theta) = p\sin\theta$, which corresponds to a rigid body rotation

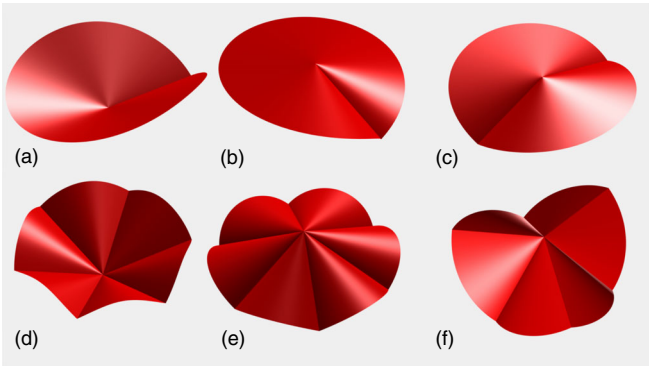

FIG. 3 (color online). Theoretical prediction of f-cone patterns corresponding to the situations shown in Fig. 1. (a)–(e) Various all-valley crease configurations extracted from Eqs. (13) and (14). (a) Semi-infinite crease configuration and (b) its snapped state. (c) Snapped state of a folded sheet. (d) A vertex with six-valley creases and (e) its snapped state. (f) The symmetric $n = 6$ alternate mountain-valley crease configuration [see Eq. (21)].

of the plate around the crease. On the other hand, the snapped state with two nonaligned creases is in tension ($\lambda_2^- = -2.41$). These two states have, respectively, the energy densities per face $\mathcal{E}_2^+ = 0$ as expected from a bending-free state and $\mathcal{E}_2^- = 4.26(Bp^2/2\rho)$ for the snapped state shown in Fig. 3(c).

Furthermore, the deflections $\psi_n^\pm$ for $n > 2$ undergo hoop stresses with opposite signs: ψ_n^+ structures are in compression while ψ_n^- structures are in tension. This property is verified experimentally [13]: if cut along an arbitrary radius, ψ_n^+ collapses while ψ_n^- opens up, while for $n = 1$, both structures open up. Examples of these structures are shown in Figs. 3(d) and 3(e).

Let us now focus on the behavior of these structures for a large number of faces. Developing the inextensibility condition (3) for large n yields the following asymptotic solutions:

$$\mu_n^\pm = \frac{3^{1/4}\sqrt{n}}{\sqrt{\pi}} + O\left(\frac{1}{\sqrt{n}}\right). \tag{15}$$

Injecting this expression in the energy density per face and developing in the large n limit yields

$$\mathcal{E}_n^\pm = \frac{Bp^2}{2\rho}\left[\frac{2n}{\pi} \mp \frac{4}{\sqrt{3}} + O\left(\frac{1}{n}\right)\right]. \tag{16}$$

This energy density is asymptotically linear in n, which is consistent with the fact that the radius of the curvature of each face scales with its angular width. Consequently, the energy density of the whole structure scales as n^2 for a large number of faces.

Alternate creases f cone.— A natural extension of this analysis consists in considering a structure in which the creases are alternatively valleys and mountains, resulting in a generalized origami vertex where face bending is allowed. In this alternate creases configuration, the boundary conditions (7) read

$$\psi'(0) = p, \qquad \psi'(\phi) = \epsilon p, \tag{17}$$

where the local slopes for the valley ($\theta = 0$) and the mountain ($\theta = \phi$) creases are allowed to be proportional by a factor ϵ. We investigate configurations with $0 \le \epsilon \le 1$, since the configurations with $\epsilon' = 1/\epsilon \ge 1$ are obtained by flipping the structure upsidedown and rotating it around the z axis by an angle ϕ. Solving Eq. (6) with boundary conditions (8) and (17) yields

$$\psi(\theta) = p\frac{\cos\mu(\theta-\phi) - \epsilon\cos\mu\theta}{\mu\sin\mu\phi}. \tag{18}$$

The inextensibility condition (3) now reads

$$\mu(1-\mu^2)\phi(1+\epsilon^2-2\epsilon\cos\mu\phi) = (1+\mu^2)[2\epsilon-(1+\epsilon^2)\cos\mu\phi]. \quad (19)$$

This equation also admits solutions $\mu_n^+(\epsilon)$ and $i\mu_n^-(\epsilon)$ ($\mu_n^\pm \geq 0$), which are represented in Fig. 4. The two branches correspond to the two possible shapes of this generalized problem.

First we notice that all branches collapse to $\lambda = -1$ at $\epsilon = 1$ that corresponds to equal mountain and valley crease angles. More precisely, the expansion of Eq. (19) in terms of $(1-\epsilon)$ yields

$$\lambda_n^\pm = -1 \pm \frac{n(1-\epsilon)}{2\pi\sqrt{1-\frac{1}{3}\left(\frac{\pi}{n}\right)^2}} + O((1-\epsilon)^2). \quad (20)$$

Using this result, one finds that within the limit $\epsilon \to 1$, Eq. (18) admits simple asymptotic expressions

$$\psi_n^\pm(\theta) = p\left(\theta - \frac{\pi}{n} \pm \sqrt{1-\frac{1}{3}\left(\frac{\pi}{n}\right)^2}\right). \quad (21)$$

In particular, these two states are obtained from one another by mirror symmetry about the $z=0$ plane followed by a rotation of angle ϕ. The corresponding shape is shown in Fig. 3(f). The energy density per face for this structure reads

$$\mathcal{E}_n = \frac{Bp^2}{2\rho}\frac{2\pi}{n}. \quad (22)$$

The total energy density is, thus, independent of n, in sharp contrast with the all-valley creases structures.

Interestingly, $\lambda_n^\pm$ admit finite limits as $\epsilon \to 0$. In this limit, each mountain crease disappears from the corresponding structures and is replaced by a local extremum. The corresponding structures, hence, match exactly the $n/2$ all-valley creases f cone. These values of λ are, thus, given by the corresponding values of $\mu_{n/2}^\pm$ shown in Fig. 2. In particular, we recover the two tensile states for $n=2$ which correspond to the semi-infinite crease configurations studied above, and the infinite crease state for $n=4$.

Finally, for all $n \geq 4$, hoop-stress-free ($\lambda = 0$) configurations are achieved for a finite value of $\epsilon = \epsilon_n^0$ given by

$$\epsilon_n^0 = \frac{\sin\left(\frac{\pi}{4}-\frac{\pi}{n}\right)}{\sin\left(\frac{\pi}{4}+\frac{\pi}{n}\right)}. \quad (23)$$

The deflection for the corresponding structures reads

$$\psi_n^+ = p\frac{\sin\left(\theta+\frac{\pi}{4}-\frac{\pi}{n}\right)}{\sin\left(\frac{\pi}{4}+\frac{\pi}{n}\right)}. \quad (24)$$

These configurations carry vanishing bending energy and are, thus, flat faced. In fact, Eqs. (23) and (24) provide the kinematics and shape of deployable mechanisms with rigid faces, where the deployment is provided by changing the slope p. However, in the present case, the faces are not rigid, and, instead, the crease slope is fixed. Thus, these flat-faced configurations will snap into tensile ψ_n^- configurations with bent faces and nonzero hoop stress obtained by picking the value from the other branch λ_n^- at ϵ_n^0. As can be seen in Fig. 4, such flat-faced configurations do not exist for $n=2$ ($\lambda_2^\pm < 0$), while for $n=4$, the two mountain creases disappear from the flat-faced state ($\epsilon_4^0 = 0$). The structures discussed in this section are displayed in Fig. 5.

Imprinting evenly distributed radial creases on a thin sheet results in the appearance of two metastable states corresponding to structures that can be snapped through one another. We fully characterized these patterns when the creases are infinitely rigid and either all-valley or alternatively valley and mountain. This latter case admits symmetric metastable states when the mountain and valley crease angles are identical and also yields the kinematics of flat-faced origami vertices when these angles are chosen

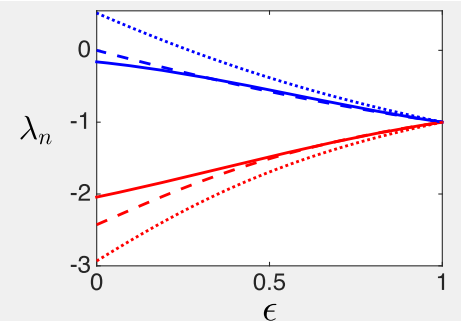

FIG. 4 (color online). Lagrange multipliers λ_n^+ (blue curves) and λ_n^- (red curves) solutions of the inextensibility condition (19) for the alternate creases f cone as a function of the crease angle ratio ϵ for $n=2$, 4, 6 creases (respectively, plain, dashed, and dotted lines).

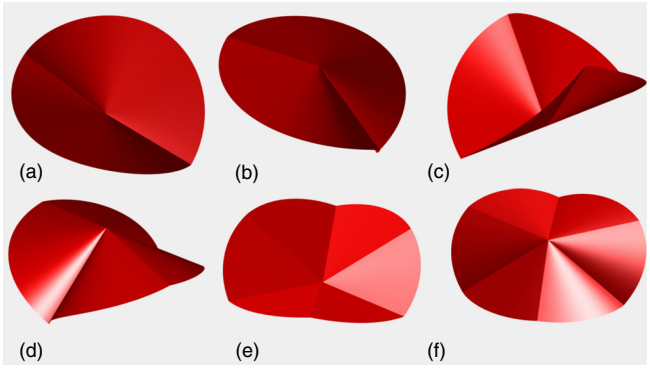

FIG. 5 (color online). f cones for alternate mountain-valley creases for a different number of creases n. The different configurations are deduced from Eqs. (18) and (19). (a) $n=2$ and (b) its snapped state; (c) $n=4$ and (d) its snapped state. The ratio of the mountain and valley opening angles is $\epsilon = 0.2$. Note that these states are forbidden if the faces are rigidly flat. (e) $n=6$ flat-faced configuration given by Eq. (24) and (f) its corresponding snapped curved state.

adequately. These structures admit straightforward experimental realizations even when the scale separation between L^* and the system size R is rather weak (see Fig. 1). The energetic properties and shapes described here are, thus, robust as soon as a large-scale separation between thickness and system size is achieved.

Finally, for a connected network of creases, the faces would generally bend as soon as they are bounded by more than four creases, though at a higher bending energy cost [15]. Imprinting patterns on an elastic sheet will, in practice, modify its shape and its local mechanical properties [8]. f cones can be seen as a simplified model for building blocks of functional crease networks aimed to provide modularity in the shape and the mechanical response of origami-based shell-like structures, such as Resch patterns [16]. We expect that the overall shape of general crease networks and local stability properties strongly depend on the spatial distribution of the creases' rest angles and stiffnesses [17]. Experimentally, bistability is a robust property within these extended structures. In particular, the snapping of a vertex locks the local kinematics into a deployed state and, thus, acts as a mechanical switch.

The authors thank S. Moulinet and B. Thiria for fruitful discussions. This research was supported by the Grant No. ANR-14-CE07-0031 METAMAT.

[1] E. D. Demaine, Ph.D. thesis, University of Waterloo, 2001.
[2] M. Schenk and S. D. Guest, Proc. Natl. Acad. Sci. U.S.A. **110**, 3276 (2013).
[3] Z. Y. Wei, Z. V. Guo, L. Dudte, H. Y. Liang, and L. Mahadevan, Phys. Rev. Lett. **110**, 215501 (2013).
[4] S. Waitukaitis, R. Menaut, B. Gin-ge Chen, and M. van Hecke, Phys. Rev. Lett. **114**, 055503 (2015).
[5] K. Miura, in *Research of Pattern Formation*, edited by R. Takaki (KTK Scientific Publishers, Tokyo, 1994), pp. 77–90.
[6] M. Schenk, A. D. Viquerat, K. A. Seffen, and S. D. Guest, J. Spacecr. Rockets **51**, 762 (2014).
[7] B. Thiria and M. Adda-Bedia, Phys. Rev. Lett. **107**, 025506 (2011).
[8] J. L. Silverberg, A. A. Evans, L. McLeod, R. C. Hayward, T. Hull, C. D. Santangelo, and I. Cohen, Science **345**, 647 (2014).
[9] M. Ben Amar and Y. Pomeau, Proc. R. Soc. A **453**, 729 (1997).
[10] T. A. Witten, Rev. Mod. Phys. **79**, 643 (2007).
[11] M. M. Müller, M. Ben Amar, and J. Guven, Phys. Rev. Lett. **101**, 156104 (2008).
[12] F. Lechenault, B. Thiria, and M. Adda-Bedia, Phys. Rev. Lett. **112**, 244301 (2014).
[13] See the Supplemental Material at http://link.aps.org/supplemental/10.1103/PhysRevLett.115.235501 for the general vertex solution and an experimental illustration of the hoop stress undergone by the f cone.
[14] E. Cerda and L. Mahadevan, Phys. Rev. Lett. **80**, 2358 (1998).
[15] J. L. Silverberg, J.-H. Na, A. A. Evans, B. Liu, T. C. Hull, C. D. Santangelo, R. J. Lang, R. C. Hayward, and I. Cohen, Nat. Mater. **14**, 389 (2015).
[16] T. Tachi, Journal of mechanical design **135**, 111006 (2013).
[17] V. Brunck, F. Lechenault, A. Reid, and M. Adda-Bedia (to be published).